HETEROCYCLES, Vol. 101, No. 2, 2020, pp. 559 - 579. © 2020 The Japan Institute of Heterocyclic Chemistry
Received, 9th July, 2019, Accepted, 27th August, 2019, Published online, 2nd October, 2019
DOI: 10.3987/COM-19-S(F)47

# DEVELOPMENT OF NEAR-INFRARED FLUORESCENT PROBES WITH LARGE STOKES SHIFTS FOR NON-INVASIVE IMAGING OF TUMOR HYPOXIA

**Kensuke Okuda,[1†] Bahaa G. M. Youssif,[1,2] Ryosuke Sakai,[1] Takahiro Ueno,[1] Takayuki Sakai, [1] Tetsuya Kadonosono,[3] Yasuyuki Okabe,[1] Ola I. Abdel Razek Salem,[2] Alaa M. Hayallah,[4] Mostafa A. Hussein,[2] Shinae Kizaka-Kondoh,[3] and Hideko Nagasawa[1]***

[1] Laboratory of Pharmaceutical and Medicinal Chemistry, Gifu Pharmaceutical University, 1-25-4 Daigaku-nishi, Gifu 501-1196 Japan. E-mail: hnagasawa@gifu-pu.ac.jp

[2] Pharmaceutical Organic Chemistry Department, Faculty of Pharmacy, Assiut University, Assiut 71526 Egypt.

[3] School of Life Science & Technology, Tokyo Institute of Technology, 4259 Nagatsuta-cho, Midori-ku, Yokohama, Kanagawa 226-8501 Japan.

[4] Pharmaceutical Chemistry Department, Faculty of Pharmacy, Deraya University, Minia Egypt.

† Present affiliation: Laboratory of Bioorganic & Natural Products Chemistry, Kobe Pharmaceutical University, 4-19-1 Motoyama-kita, Higashinada, Kobe 658-8558 Japan.

**Abstract** – A series of near-infrared (NIR) fluorochromes with large Stokes shifts was designed, synthesized, and evaluated for application in non-invasive imaging of tumor hypoxia. Each NIR fluorescent hypoxia probe comprised a tricarbocyanine dye and a 2-nitroimidazole-containing moiety as a hypoxia marker that binds to cellular nucleophiles via bioreductive activation under hypoxic conditions. Nucleophilic displacement of the amino-nucleophilic linker moiety of heptamethine cyanine dyes having a 2-chloro-1-cyclohexenyl ring and a 2-nitroimidazole moiety yielded various fluorochromes with different hydrophilicity. These exhibited long emission wavelengths (747–758 nm) with large Stokes shifts (111–125 nm) and high quantum yield (0.04–0.34). GPU-210,

297, and 316 showed significantly higher levels of fluorescence under hypoxic than under normoxic conditions on treating SUIT-2/HRE-Luc pancreatic cancer cells. Among these, only GPU-316 showed significant fluorescence intensity in tumor tissue in *in vivo* fluorescence imaging of mouse xenograft models.

## INTRODUCTION

Tumor hypoxia is now known as an important factor that negatively influences the prognosis of cancer patients.[1,2] Hypoxic tumor cells are not only resistant to ionizing radiation and many chemotherapeutic agents but also metastasize to distant organs.[3] Therefore, there has been a growing impetus to develop non-invasive imaging methods to detect and assess tumor hypoxia.[4,5]

Nitroimidazole compounds conjugated with a radionuclide function as hypoxia markers and have been used for non-invasive imaging of tumor hypoxia.[6] For example, pimonidazole is widely used as a hypoxia marker for immunohistochemical analysis (Figure 1).[7] These compounds are known to be selectively trapped in hypoxic tissue via enzymatic reduction of the nitro group to form anion radicals that are further reduced in the absence of oxygen. Although several radiopharmaceuticals with a nitroimidazole group are in clinical use, current radionuclide imaging methods have poor spatial and temporal resolution and are subject to stringent safety regulations that limit their repeated use.[8,9]

Optical imaging, however, has comparable sensitivity to that of radionuclide imaging and can be employed if the emitting fluorophore is conjugated to a targeting ligand. It is safer and easier to perform than nuclear imaging.[10] Optical imaging in the NIR region (650–900 nm) involves low absorption by intrinsic photoactive biomolecules and allows light to penetrate a few centimeters into the tissue, a sufficient depth for imaging practically all small animal models.[11] Therefore, NIR fluorescence imaging, a less expensive and non-invasive technique, may be a powerful tool for imaging tumor hypoxia. Motivated by the aforementioned facts, we developed a NIR hypoxia probe, GPU-167 (Figure 1), comprising two pimonidazole moieties and a tricarbocyanine dye, for *in vivo* imaging of tumor hypoxia.[12] This is the first chemical probe to visualize tumor hypoxia by NIR fluorescence with a significant tumor-to-background (T/B) ratio (muscle as the reference tissue) in a mouse xenograft model. However, the presence of diastereomers of GPU-167, due to its two chiral carbons, hinder its synthesis and further elaboration and its pharmacokinetics and tumor distribution require improvement. We also synthesized GPU-311 as another achiral candidate for a hypoxia-selective NIR fluorochrome (Figure 1).[13] The heptamethine cyanine dye used has a cyclohexenyl ring moiety that increases its photostability[14] and provides a chemically reactive site for nucleophilic substitution at the center methine carbon of the dye.[15] A sulfur nucleophile was utilized to couple tricarbocyanine and a 2-nitroimidazole moiety with a hydrophilic tetraethylene glycol linker. Evaluation of its hypoxia selectivity *in vitro* was promising;

however, *in vivo* fluorescence imaging of a mouse xenograft model after GPU-311 administration revealed inadequate accumulation of GPU-311 in tumors due to its rapid elimination by the liver. Another potential drawback of GPU-167 and 311 was their small Stokes shifts (25 and 17 nm, respectively), which can cause self-quenching and measurement errors due to excitation light and scattered light. Therefore, we designed a new molecule, inspired by the fact that direct attachment of the alkylamine to the cyclohexene ring of heptamethine cyanine dramatically increases the Stokes shift.[16] Here we report on the design, synthesis, and functional evaluation of hypoxia-selective NIR probes with large Stokes shifts for non-invasive imaging of tumor hypoxia.

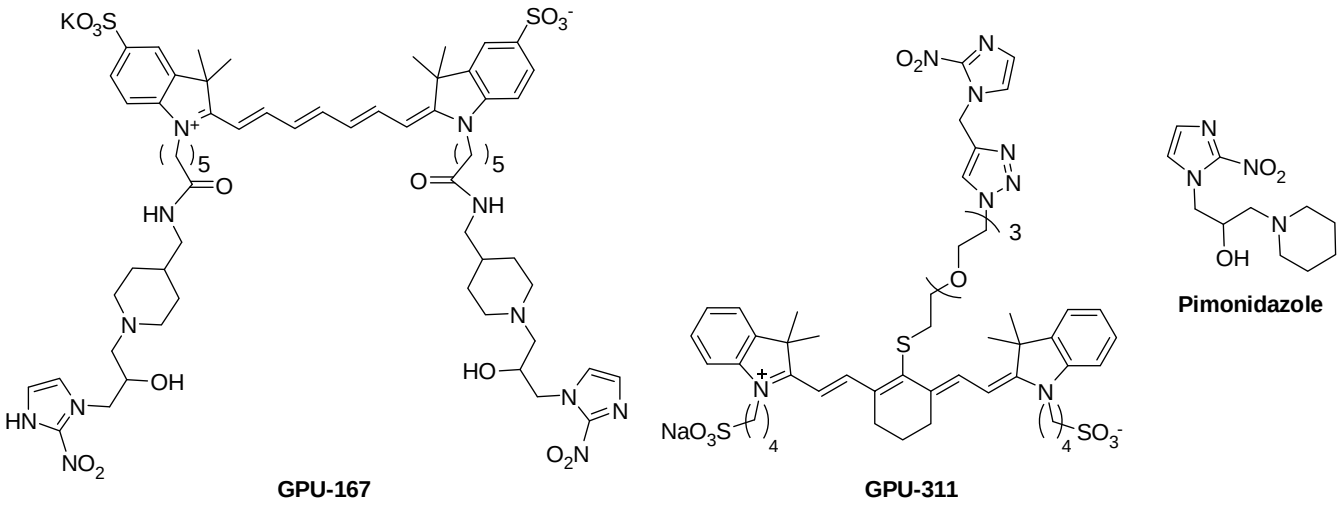


**Figure 1.** Structures of GPU-167, GPU-311, and pimonidazole

## RESULTS AND DISCUSSION

**Molecular Design** The molecular design depends on conjugation of the 2-nitroimidazole derivative as a hypoxia targeting moiety and a NIR fluorescent dye with a cyclohexene moiety through different linkers (Figure 2). It is known that introducing cyclohexene rings into the methine bridges of heptamethine cyanine dyes increases their rigidity and stability, resulting in high quantum yields.[17]

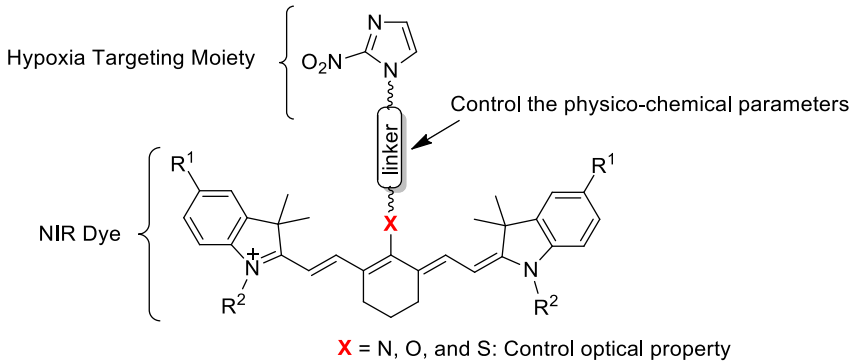


**Figure 2.** Molecular design of NIR fluorescent probe for hypoxia imaging

Therefore, we chose two different known NIR fluorescent precursors containing chlorocyclohexyl moieties in the polyene chain of a functionalized cyanine dye, compound **1**[18] with alkyl sulfonate groups for GPU-172, 210, 297, and 298 and compound **2**[19] with aryl sulfonate groups for GPU-316, 309, and 310, respectively (Figure 3). The linker should affect the pharmacokinetics and biodistribution, accumulation,

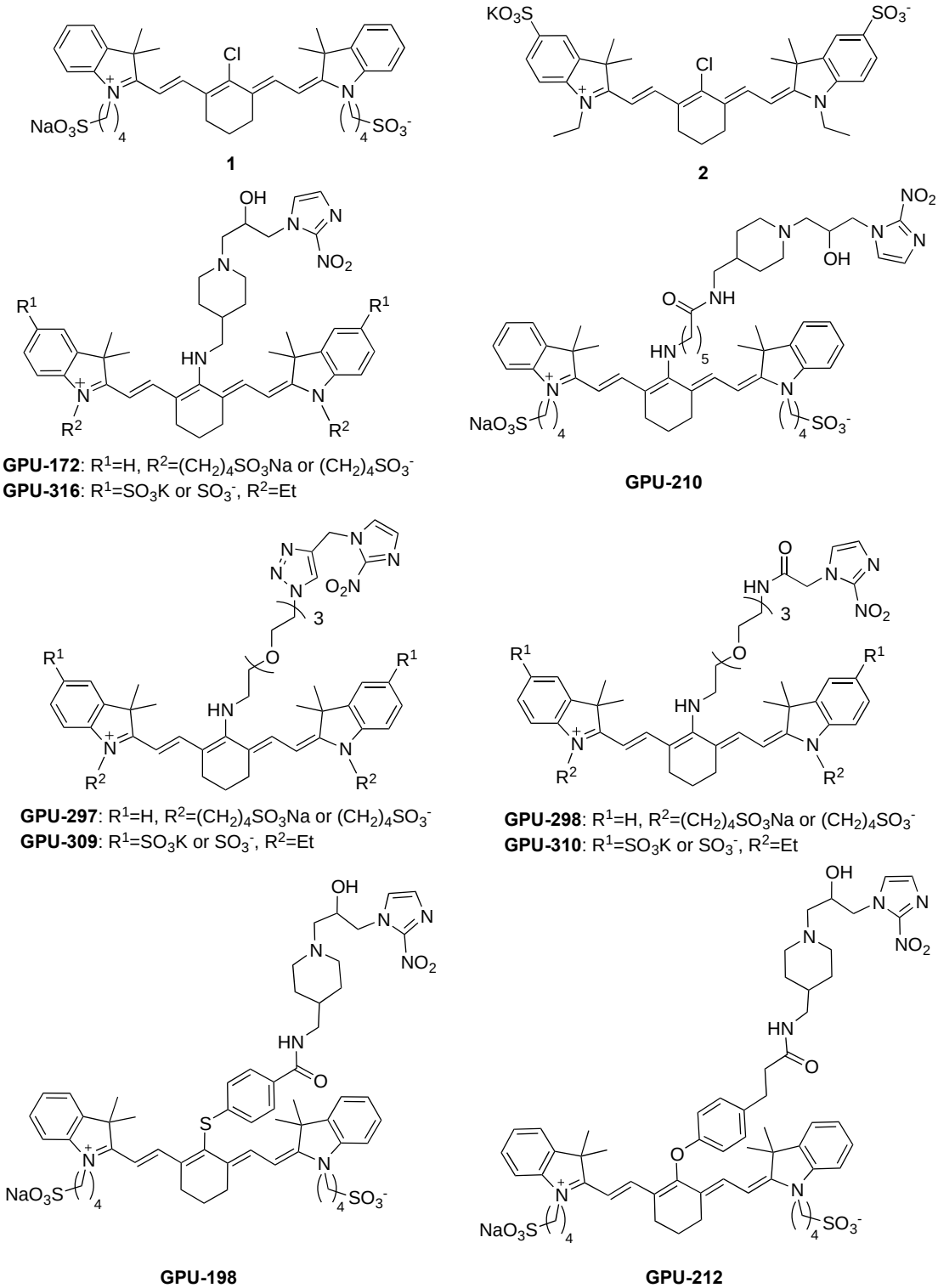


**Figure 3.** Structures of NIR fluorescent probes

duration of retention in the target organ, and rapidity of clearance from untargeted sites by control of the physicochemical properties, as seen in developing the antibody-drug conjugate.[20] The hydrophilicity and solubility were adjusted by linkers with different polarities, i.e., alkylene or polyethylene glycol linkers. The linker moieties were introduced by $S_{RN}1$ reaction with nitrogen nucleophiles on the methine bridge of tricarbocyanine dyes to obtain large Stokes shifts.[16,21] We also prepared other heteroatom-linked fluorescent probes containing S or O atoms to verify the effect of N as a bridging atom on the photophysical properties (GPU-198 and 212).

**Synthesis** First, tricarbocyanine precursors **1**[18] and **2**[19] were prepared according to literature procedures for further elaboration with the 2-nitroimidazole moiety. These precursors have a chlorine atom at the *meso* position, which can be easily replaced by various nucleophiles through an $S_{RN}1$ mechanism.[15,16,18,19,21]

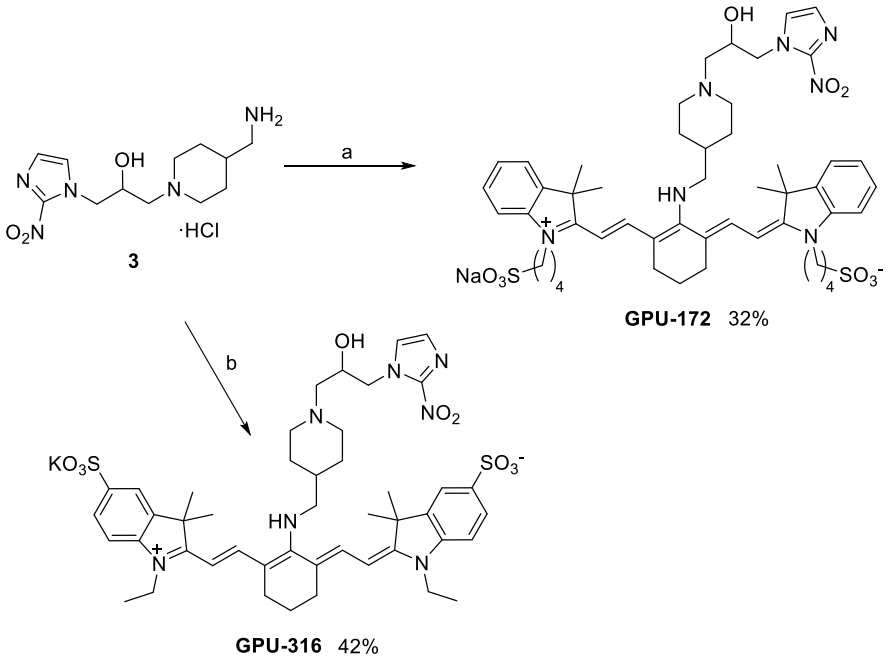


**Scheme 1.** Reagents and conditions: (a) **1**, DMF, 85 °C, 3.5 h; (b) **2**, $Et_3N$, DMF, 80 °C, 3 h

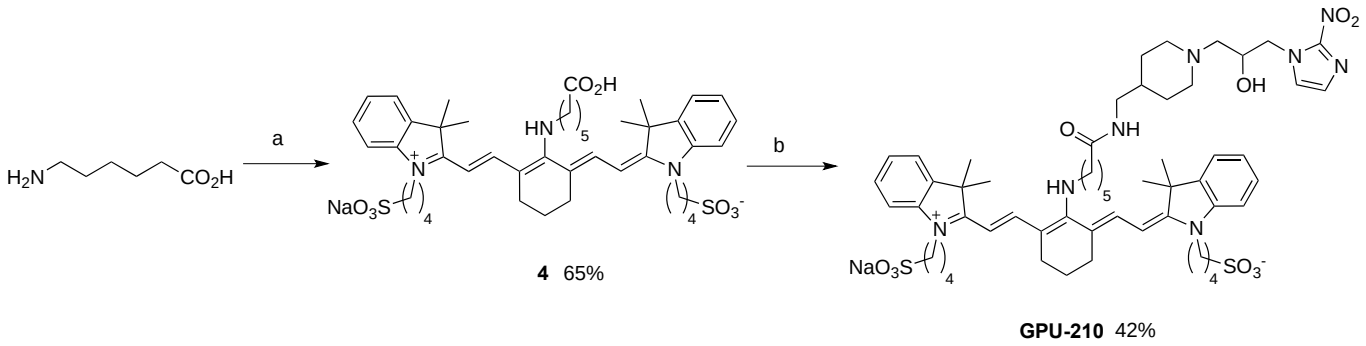


**Scheme 2.** Reagents and conditions: (a) **1**, DMF, 85 °C, 3.5 h; (b) EDCI·HCl, HOBt·$H_2O$, DMF, rt, 30 min then **3**, rt, 20 h

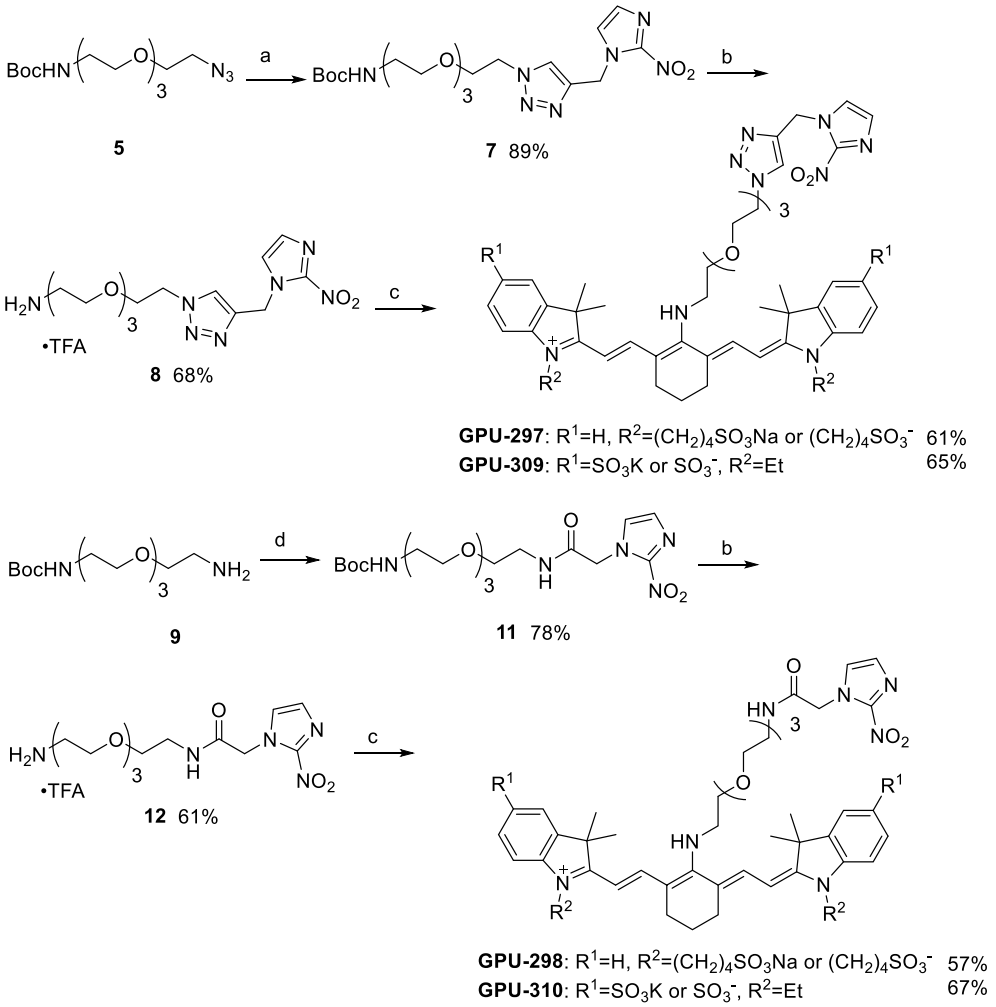


**Scheme 3.** Reagents and conditions: (a) 2-nitro-1-(prop-2-ynyl)-1*H*-imidazole (**6**), $Cu(OAc)_2$, sodium L-ascorbate, *t*-BuOH/$H_2O$, rt, 20 h; (b) $CH_2Cl_2$/TFA, rt, 45 min; (c) **1** or **2**, DMF, 80 °C, 4 h; (d) CDI, DMF, rt, 45 min then 2-(2-nitro-1*H*-imidazol-1-yl)acetic acid (**10**), rt, 18 h

Next, GPU-172 and GPU-316 were synthesized as illustrated in Scheme 1. Nucleophilic substitution at the central vinyl halide carbons of **1** and **2** by **3**[12] at an elevated temperature provided the final products, GPU-172 and GPU-316, respectively. This reaction was conveniently monitored by a color change in the reaction solution. Specifically, completion of the reaction was indicated by a color change from green to blue, corresponding to a hypochromic shift of the dye. It is noteworthy that this reaction did not occur at room temperature, as did a similar previous reported amine substitution reaction.[16] We then started to prepare GPU-210 as shown in Scheme 2. Replacing the *meso*-chlorine atom in **1** by a nucleophilic amino group of 6-aminohexanoic acid at an elevated temperature provided key intermediate **4** in moderate yield (65%). Conjugation of **4** with **3** using 1-ethyl-3-(3-dimethylaminopropyl)carbodiimide hydrochloride (EDCI·HCl) in the presence of a catalytic amount of 1-hydroxybenzotriazole (HOBt) monohydrate afforded GPU-210 in 42% yield.

We then attempted to prepare GPU-297, 298, 309, and 310 as shown in Scheme 3. We used Hüisgen cycloaddition and amide bond formation to form a reliable connection between the 2-nitroimidazole and linker moieties. Moreover, triazole and/or amide can achieve more than just linking because they can readily associate with biological targets through hydrogen bonding and dipole interactions.[22] For Hüisgen cycloaddition, Cu(I)-catalyzed 1,3-dipolar cycloaddition of **5**[23] with **6**[24] using $Cu(OAc)_2$ and sodium L-ascorbate in a mixture of 1:1 *t*-BuOH/$H_2O$ furnished **7** in 89% yield. The Boc group in **7** was removed using a mixture of $CH_2Cl_2$/TFA (4:1, v/v) to obtain **8** in 68% yield. Then, for the amide bond linkage, **9**[25] was activated with carbonyldiimidazole (CDI) in anhydrous DMF to form the acyl imidazole intermediate *in situ* followed by coupling with **10**[26] to give **11** in 78% yield. The Boc-group in **11** was deprotected using the same procedure as for the synthesis of **8** to give compound **12** in 61% yield. These hydrophilically tethered linkers conjugated to hypoxia targeting moieties (**8** or **12**) were then conjugated to NIR dyes (**1** or **2**) by replacing the *meso*-chlorine atom in cyanine **1** or **2** by an amino group of compound **8** or **12** at an elevated temperature to give probes GPU-297, 298, 309, and 310 in 57%–67% yields. Finally, GPU-198 and 212, in which fluorescent dyes and hypoxic marker moieties were linked via an S or O atom, were synthesized as shown in Scheme 4.

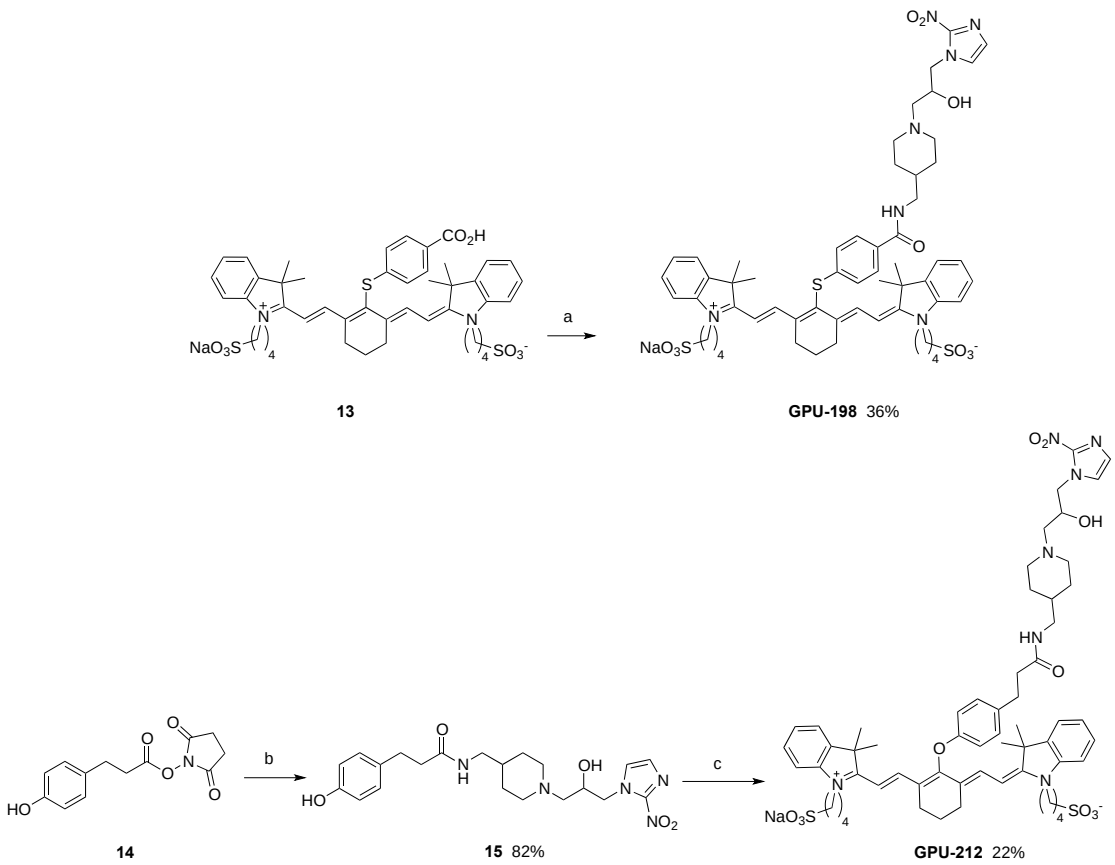


**Scheme 4.** Reagents and conditions: (a) (i) HOSu, DIC, DMAP, DMF, rt, 24 h, (ii) **3**, DIPEA, DMF, rt, 24 h; (b) **3**, DMF, rt, 20 h; (c) NaH, DMF, rt, 30 min, then **1**, rt, 1 h

Compound **13**[27] was reacted with *N*-hydroxysuccinimide (HOSu) in the presence of *N*,*N*'-diisopropylcarbodiimide (DIC) to give an activated ester intermediate, which was directly conjugated with the amino group of **3** to give GPU-198 in 36% yield. Compound **14**[28] was reacted efficiently with compound **3** to give compound **15** in 82% yield. Etherification of **15** with dye **1** was achieved in the presence of NaH/DMF to afford probe GPU-212 in 22% yield. Analytical HPLC was performed to assess the purity of the products (see Supplementary data for details).

**Spectral Analysis** We first compared the absorption and fluorescence spectra of GPU-172, 316, 210, 297, 309, 298, 310, 198, and 212 in methanol (Table 1). All GPU dyes displayed strong absorption with high molar absorption coefficients reaching $10^5$ $L \cdot M^{-1} \cdot cm^{-1}$ in methanol solutions. All exhibited NIR fluorescence (>740 nm) with quantum yields of 0.04–0.34. As expected, GPU-172, 316, 210, 297, 309, 298, and 310 exhibited large Stokes shifts (111–125 nm).[16] Conversely, GPU-198 and 212 showed small Stokes shifts (<20 nm). Thus, it was confirmed for our compounds that the *meso*-nitrogen functional group of the heptamethine cyanine dye causes large Stokes shifts. These are attributed to excited-state intramolecular charge transfer (ICT) from the donor nitrogen group to the acceptor heptamethine cyanine group in the dyes as described by Peng *et al*.[16]

**Table 1.** Photophysical characteristics and Rm values of probes GPU-172, 316, 210, 297, 309, 298, 310, 198, and 212

| Compound | Absorption max (nm) | Emission max (nm) | ε ($L \cdot M^{-1} \cdot cm^{-1}$) | Stokes shift (nm) | Φfl | Rm |
|---|---|---|---|---|---|---|
| GPU-172 | 639 | 756 | $4.7 \times 10^4$ | 117 | 0.041 | -0.06 |
| GPU-316 | 626 | 747 | $2.8 \times 10^4$ | 121 | 0.076 | -0.57 |
| GPU-210 | 633 | 758 | $6.7 \times 10^4$ | 125 | 0.22 | 0 |
| GPU-297 | 643 | 754 | $4.3 \times 10^4$ | 111 | 0.17 | -0.68 |
| GPU-309 | 628 | 753 | $1.6 \times 10^4$ | 125 | 0.22 | -0.62 |
| GPU-298 | 643 | 756 | $2.3 \times 10^4$ | 113 | 0.16 | -0.76 |
| GPU-310 | 631 | 756 | $4.4 \times 10^3$ | 125 | 0.34 | -0.43 |
| GPU-198 | 798 | 813 | $9.1 \times 10^4$ | 15 | 0.035 | -0.03 |
| GPU-212 | 768 | 784 | $2.6 \times 10^5$ | 16 | 0.096 | 0.14 |

**Hydrophobicity Index (Rm)** The Rm values of these GPU probes, which function as a hydrophobicity index, were measured as pharmacokinetic predictors.[29] For comparison, the Rm of indocyanine green (ICG), a clinically approved NIR fluorescent dye,[30] was also determined. ICG has a short half-life and is exclusively excreted by the liver into bile.[31] The Rm values of all compounds were determined using a

reversed-phase thin-layer chromatographic system (mobile phase: 10% 5 mM sodium phosphate buffer, pH 7.4, and 90% methanol). As shown in Table 1, probes with tetraethylene glycol linkers (GPU-297, 298, 309, and 310) had higher hydrophilicity (Rm: −0.43 ~ −0.76) than those with alkyl linkers (GPU-172, 316, 210, 198, and 212, Rm: 0.14 ~ −0.57). ICG (−0.5) has no membrane permeability and is taken up into cells via an endocytic mechanism.[32] In our previous *in vivo* hypoxia imaging studies, GPU-167 showed better biodistribution than GPU-311, while the former had a higher Rm than the latter (GPU-167: −0.26, GPU-311: −0.43).[12,13]

**Fluorescence Imaging of Hypoxic Cells** *In vitro* fluorescence assays of all NIR dyes were performed using SUIT-2/HRE-Luc pancreatic cancer cells which stably carry plasmid p5HRE-luciferase, and express firefly luciferase under the control of a HIF-dependent promoter.[33] The cells were cultured under hypoxic (0.1% $O_2$) and normoxic (21% $O_2$) conditions with probes at concentrations of 0.2, 1, 5, and/or 20 μM. Compounds other than GPU-298 and 310 exhibited significantly stronger fluorescence signals in hypoxic cells than in normoxic cells at almost all concentrations shown in Figure 4. Among these, GPU-316, 210, 297, 198, and 212, which showed a significant increase in fluorescence intensity at a concentration of 5 μM under hypoxic conditions, were further examined for *in vivo* biodistribution by fluorescence imaging.

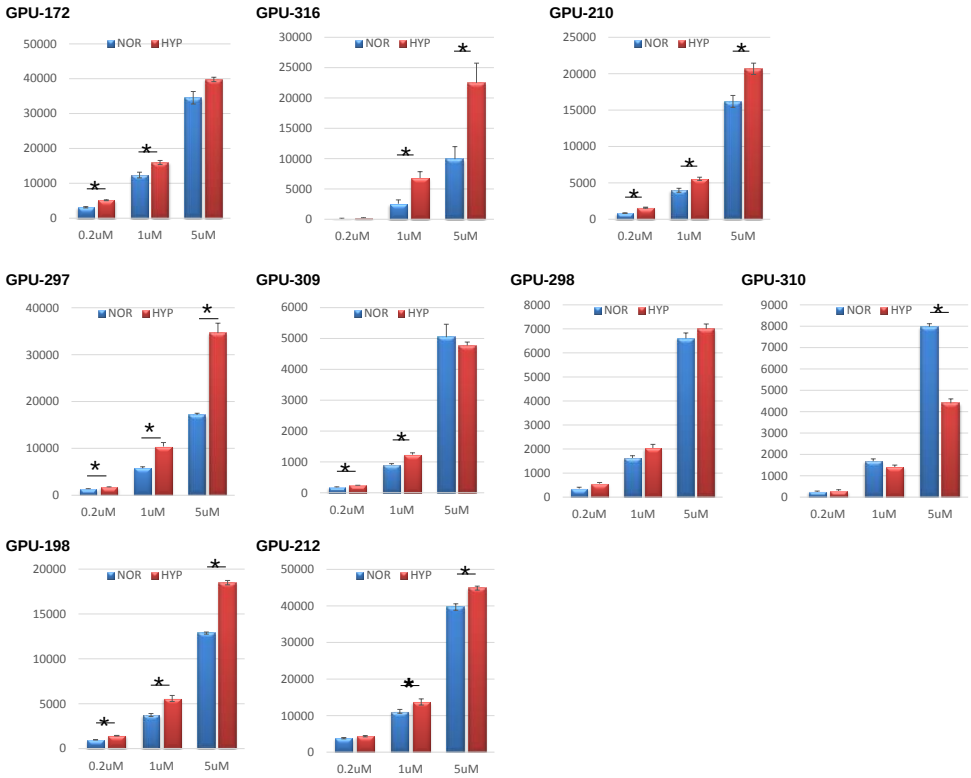


**Figure 4.** Accumulation of GPU molecules to hypoxic cells *in vitro*. The SUIT-2/HRE-Luc cells ($2 \times 10^5$ cells) cultured under normoxic (NOR) or hypoxic (HYP) conditions were treated with GPU molecules and analyzed by measurement of fluorescence intensity (*$P < 0.05$, n = 3).

***In vivo* Fluorescence Imaging of Hypoxic Tumors** The *in vivo* fluorescence imaging of hypoxic tumor cells was evaluated by intravenously injecting the above compounds into mice with subcutaneous SUIT-2/HRE-Luc tumors in the forefoot.[34] Preliminary examinations (data not shown) showed that GPU-198 was cleared in a short time, and no accumulation in the tumor was observed. Additionally, GPU-198 and 210 discolored in around two hours, suggesting that these probes would be unstable and decompose. GPU-212 was mostly excreted through the liver and kidney, and the tumor selectivity was insignificant. GPU-297 showed moderate *in vitro* hypoxia selectivity, but *in vivo*, it was mainly distributed in the liver and showed no significant accumulation in the tumor. Finally, GPU-316 showed the most promising result with *in vivo* imaging among all the compounds tested here. When GPU-316 was injected into tumor-bearing mice via the tail vein, fluorescence signals were detected throughout the body of the mice within 30 min and these gradually became weaker (Figure 5A). Signals of GPU-316 in tumors were detected as soon as 3 h after the injection and the highest T/B ratio (2.95) was obtained 12 h after injection (Figure 5B). In addition to the apparent GPU-316 accumulation in the tumors, a fluorescence signal was also detected in the abdomen. For detailed examination, we performed *ex vivo* imaging of major organs 48 h after GPU-316 administration, which revealed high fluorescence signals in the liver, spleen, and stomach and moderate signals in tumors and in the kidney (Figure 5C). In SUIT-2/HRE-Luc tumor cells, HIF-1α expression was undetectable under normoxic and severely hypoxic ($pO_2$ <10 mmHg) conditions but increased significantly under relatively mild hypoxic conditions, indicating that bioluminescence signals from SUIT-2/HRE-Luc xenografts result from HIF-active cells under relatively mild hypoxic conditions.[34] *Ex vivo* imaging of tumors at 48 h after GPU-316 injection revealed that most fluorescence signals of GPU-316 showed a similar pattern of localization to the bioluminescence signals (Figure 5D). These results demonstrate that GPU-316 efficiently detected hypoxic cells, probably adjacent to severely hypoxic regions *in vivo*. Although the significant GPU-316 accumulation in hypoxic tumors *in vivo* showed some improvement from the precedent result with GPU-311,[13] its specificity for tumor hypoxia was lower than for GPU-167.[12] For example, the highest T/B ratio for GPU-316 (3.0) was lower than that for GPU-167 (4.4), although the *in vitro* hypoxia selectivity of GPU-316 is higher than that of GPU-167 even at a lower dose.

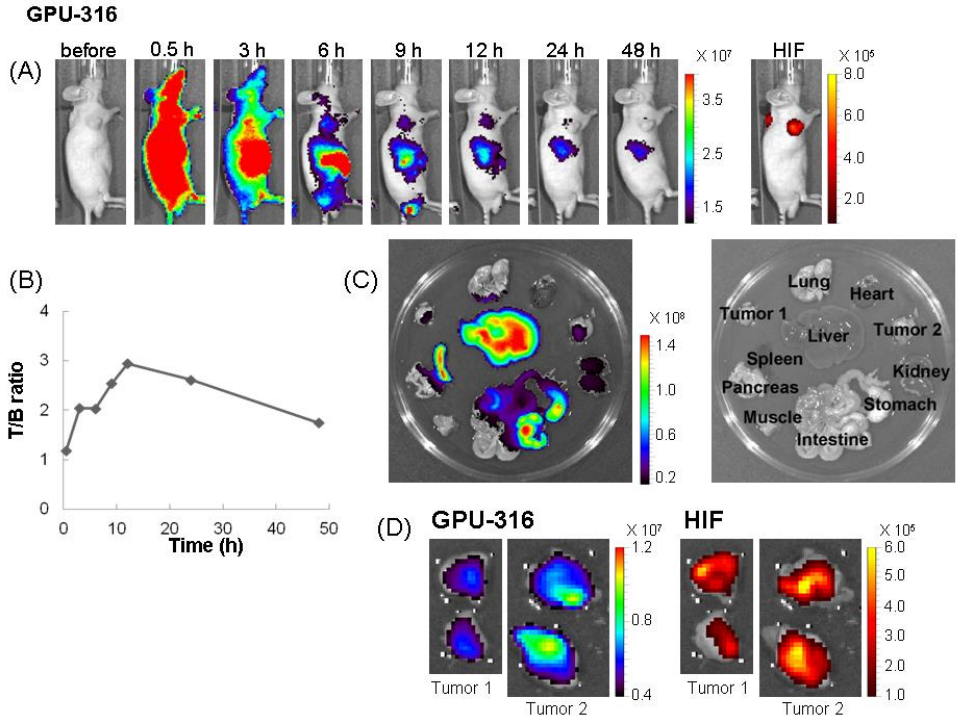


**Figure 5.** (A) *In vivo* optical imaging of hypoxic region in subcutaneous cancers with GPU-316. Representative *in vivo* images of hypoxic tumors after administration of 10 nmol of GPU-316. Nude mice carrying SUIT-2/HRE-Luc xenografts in both forefeet were imaged at the indicated time after GPU-316 injection. The right panel (HIF) shows a bioluminescence image of a HIF-1-active hypoxic tumor at 24 h. (B) Specific GPU-316 accumulation in subcutaneous xenografts. The relative fluorescence intensity for the T/B ratio is shown. Fluorescence intensities of the SUIT-2/HRE-Luc xenografts and the muscle of the hind foot were measured at the indicated time after GPU-316 administration. (C) Representative *ex vivo* fluorescence imaging of organs of hypoxic tumor bearing mouse. The mouse shown in (A) was analyzed by *ex vivo* imaging. A fluorescence image at 48 h after GPU-316 administration is shown. (D) Representative *ex vivo* fluorescence (GPU-316) and bioluminescence (HIF-1) images of excised subcutaneous tumors. The dissected tumors shown in (C) were imaged.

## CONCLUSION

In summary, we developed an efficient NIR fluorescent probe with a large Stokes shift due to ICT, GPU-316, comprising pimonidazole and tricarbocyanine dye for *in vivo* imaging of tumor hypoxia. This accumulated in tumor cells cultured under hypoxic conditions significantly more than in those cultured under normoxic conditions. We also demonstrated that hypoxic tumors were apparently visualized by NIR fluorescence with a significant T/B ratio 24 h after GPU-316 administration to living mice in a subcutaneous xenograft model.

## EXPERIMENTAL

### General Information

Unless otherwise stated, all reagents and solvents were obtained from Sigma-Aldrich (St. Louis, MO, USA), Wako Chemicals (Osaka, Japan), Nacalai Tesque (Kyoto, Japan), or Tokyo Chemical Industry (Tokyo, Japan) without further purification. Normal-phase TLC was carried out on Silica gel 60 $F_{254}$ (Merck KGaA (Darmstadt, Germany), 1.05715.0009) using reagent graded solvents. Normal-phase column chromatography was performed on silica gel (AP-300, Daikoh (Kiyosu, Japan)). Reverse-phase TLC was performed on RP-18 $F_{254S}$ (Merck KGaA, 1.15389.). All moisture or air-sensitive reactions were carried out under nitrogen atmosphere. $^1$H-NMR spectra were obtained with JEOL JNM-AL400 or JNM-EX400 spectrometer (Akishima, Japan) at 400 MHz frequency or JMN-ECA500 spectrometer at 500 MHz frequency in $CDCl_3$, $CD_3OD$, and DMSO-$d_6$ with TMS as an internal standard. Chemical shifts are reported in ppm. Coupling constants are reported in Hz. The multiplicity is defined by s (singlet), d (doublet), t (triplet), dd (doublet of doublets), br (broad), and m (multiplet). The FAB-MS measurements were carried out on a JEOL JMS-SX102A or JMS-T100TD. The Direct Analysis in Real Time (DART)-MS measurements were carried out on a JEOL JMS-T100TD. ESI-MS measurements were carried out on a Shimadzu LCMS-IT-TOF. UV-Vis spectra were obtained by a Beckman DU 640 UV-VIS spectrophotometer (Brea, CA, USA). The fluorescence excitation spectra and emission spectra were obtained by a JASCO FP-6600 Fluorescence spectrophotometer (Hachioji, Japan). The slit width was 5 nm or 10 nm for excitation and 10 nm for emission. All the newly synthesized probes were purified by Yamazen flash liquid chromatography W-Prep 2XY system (Osaka, Japan) equipped with Ultra Pack ODS-SM-50B column (26 mm I.D. × 300 mm) and their purity were analyzed by reverse phase analytical HPLC monitored at 300 nm and 630 or 640 nm absorption.

### Synthesis

Tricarbocyanine dye **1**,[18] **2**,[19] 1-[4-(aminomethyl)piperidin-1-yl]-3-(2-nitro-1*H*-imidazol-1-yl)propan-2-ol hydrochloride (**3**),[12] *tert*-butyl *N*-(2-{2-[2-(2-azidoethoxy)ethoxy]ethoxy}ethyl)carbamate (**5**),[23] 2-nitro-1-(prop-2-ynyl)-1*H*-imidazole (**6**),[24] *tert*-butyl *N*-(2-{2-[2-(2-aminoethoxy)ethoxy]ethoxy}ethyl)-carbamate (**9**),[25] 2-(2-nitro-1*H*-imidazol-1-yl)acetic acid (**10**),[26] compound **13**,[27] and 2,5-dioxopyrrolidin-1-yl 3-(4-hydroxyphenyl)propanoate (**14**)[28] were prepared according to the literature procedures.

**Tricarbocyanine GPU-172:** Compound **3**[12] (280 mg, 0.876 mmol) was added to a solution of **1**[18] (150 mg, 0.200 mmol) in DMF (5 mL). The resulting solution was stirred at 85 °C for 3.5 h. After the solvent was removed, the residue was dissolved in MeOH (2 mL) and precipitated by $Et_2O$ (25 mL). The solid was collected by centrifugation and was further purified with RP-MPLC using $H_2O$/MeCN as an eluent to give GPU-172 (63.8 mg, 32%) as a dark blue solid. $^1$H-NMR (DMSO-$d_6$, 400 MHz): δ 7.60 (d, $J$=12.9

Hz, 2H), 7.52 (d, *J*=1.0 Hz, 1H), 7.40 (d, *J*=7.1 Hz, 2H), 7.27 (t, *J*=7.4 Hz, 2H), 7.13 (d, *J*=7.8 Hz, 2H), 7.10 (d, *J*=0.7 Hz, 1H), 7.04 (t, *J*=7.4 Hz, 2H), 5.80 (d, *J*=12.0 Hz, 2H), 5.01 (1H, d, *J*=5.9 Hz, 1H), 4.67 (dd, *J*=13.3, 3.0 Hz, 1H), 4.21 (dd, *J*=13.4, 7.8 Hz, 1H), 4.02–3.86 (m, 4H), 3.57 (d, *J*=4.9 Hz, 2H), 2.92 (d, *J*=11.0 Hz, 1H), 2.80 (d, *J*=12.0 Hz, 1H), 2.54 (br, 7H), 2.33 (dd, *J*=13.0, 5.4 Hz, 1H), 2.24 (dd, *J*=12.8, 7.5 Hz, 1H), 2.03 (t, *J*=10.7 Hz, 1H), 1.94 (t, *J* = 10.9 Hz, 1H), 1.84–1.66 (m, 14H), 1.60 (s, 12H), 1.31–1.10 (m, 2H); HR-ESI-MS *m/z*: 972.4361 ([M-Na]$^-$, calcd for $C_{50}H_{67}N_7O_9S_2$: 972.4369).

**Tricarbocyanine GPU-316:** To a stirring solution of **2** (25.0 mg, 0.0352 mmol) dissolved in DMF (5 mL) was added **3** (50.0 mg, 0.156 mmol). To a stirring the resulting solution was slowly added in drops $Et_3N$ (24.5 μL, 0.176 mmol), the resulting solution was stirred at 80 °C for 3 h. After cooling, the solvent was removed under reduced pressure. To the residue was added $Et_2O$ (15 mL) and the resulting precipitate was collected by centrifugation. After the solvent was removed, the residue was dissolved in MeOH and evaporated. The solid was purified with RP-MPLC using $H_2O$/MeCN as eluent to give GPU-316 (14.1 mg, 42%) as a dark blue solid. $^1$H-NMR (DMSO-*d*$_6$, 400 MHz): δ 8.57 (br s, 1H), 7.68–7.5 (m, 7H), 7.19 (s, 1H), 7.08 (d, *J*=8.2 Hz, 2H), 5.81 (br d, *J*=12.1 Hz, 2H), 4.55 (br d, *J*=10.3 Hz, 1H), 4.32 (br, 1H), 4.12 (q, *J*=5.2 Hz, 1H), 4.00 (br q, *J*=6.1 Hz, 4H), 3.59 (br, 2H), 3.17 (d, *J*=4.6 Hz, 1H), 3.10 (q, *J*=7.3 Hz, 1H), 2.54 (s, 1H), 2.50 (br, 8H), 1.79–1.69 (m, 2H), 1.59 (s, 12H), 1.21 (t, *J*=7.1 Hz, 6H), 1.24–1.13 (m, 2H). HR-ESI-MS *m/z*: 916.3703 ([M-K]$^-$, calcd for $C_{46}H_{59}N_7O_9S_2$: 916.3743).

**Tricarbocyanine 4:** To a solution of **1** (150 mg, 0.200 mmol) in DMF (5 mL), 6-aminohexanoic acid (130 mg, 0.991 mmol) was added. The resulting solution was stirred at 85 °C for 3.5 h. After the solvent was removed, the residue was dissolved in MeOH (2 mL) and precipitated by $Et_2O$ (25 mL). The solid was collected by centrifugation and was filtered and further purified with RP-MPLC using $H_2O$/MeOH as an eluent to give **4** (110 mg, 65%) as a dark blue solid. $^1$H-NMR (DMSO-*d*$_6$, 400 MHz): δ 8.18 (s, 2H), 7.49 (d, *J*=11.5 Hz, 2H), 7.31 (d, *J*=7.3 Hz, 2H), 7.23 (t, *J*=7.7 Hz, 2H), 7.05–6.95 (m, 4H), 5.68 (d, *J*=10.9 Hz, 2H), 3.87 (br, 4H), 3.67 (br t, *J*=6.0 Hz, 2H), 2.61 (br t, *J*=5.8 Hz, 4H), 2.51 (br t, *J*=6.6 Hz, 4H), 2.09 (t, *J*=7.0 Hz, 2H), 1.85–1.69 (m, 12H), 1.60 (s, 12H), 1.60–1.50 (m, 2H), 1.47–1.35 (m, 2H); FAB-MS *m/z*: 822 ([M+2H-Na]$^+$), 844 ([M+H]$^+$).

**Tricarbocyanine GPU-210:** To a solution of **4** (60.0 mg, 0.0711 mmol) in DMF (5 mL), EDCI·HCl (48.0 mg, 0.250 mmol), and HOBt·$H_2O$ (2.0 mg, 0.013 mmol) were added. The mixture was stirred at room temperature for 30 min. After that, a solution of **3** (15.0 mg, 0.0469 mmol) in DMF (1 mL) was added and the resulting mixture was stirred at room temperature for 20 h. After the solvent was removed, the residue was dissolved in MeOH (2 mL) and precipitated by $Et_2O$ (25 mL). The solid was collected by centrifugation and was further purified with RP-MPLC using 0.1 M $Et_3N$/AcOH buffer (pH 7.3)/MeCN as an eluent to give GPU-210 (22.0 mg, 42%) as a dark blue solid. $^1$H-NMR (DMSO-*d*$_6$, 500 MHz):

δ 8.33 (s, 1H), 7.81 (br m, 1H), 7.59 (s, 1H), 7.57 (s, 2H), 7.42 (d, *J*=7.2 Hz, 2H), 7.28 (t, *J*=7.6 Hz, 2H), 7.19–7.11 (m, 3H), 7.04 (t, *J*=7.3 Hz, 2H), 5.80 (d, *J*=11.6 Hz, 2H), 4.66 (dd, *J*=13.6, 2.3 Hz, 1H), 4.20 (dd, *J*=14.0, 8.0 Hz, 1H), 3.95 (br s, 5H), 3.68 (br t, *J*=6.5 Hz, 2H), 2.70 (d, *J*=12.1 Hz, 1H), 2.57–2.43 (m, 10H), 2.31–2.17 (m, 2H), 2.07 (t, *J*=7.3 Hz, 2H), 1.81–1.62 (br m, 16H), 1.59 (s, 12H), 1.61–1.44 (m, 4H), 1.38–1.25 (m, 4H). HR-ESI-MS *m/z*: 1078.5393 ([M+2H-Na]$^+$, calcd for $C_{56}H_{78}N_8O_{10}S_2$: 1078.5355).

***tert*-Butyl (11-{4-[(2-nitro-1*H*-imidazol-1-yl)methyl]-1*H*-1,2,3-triazol-1-yl}-3,6,9-trioxaundecyl)-carbamate (7):** To a solution of **6**[24] (310 mg, 2.05 mmol) in a mixture of *t*-BuOH (3 mL) and $H_2O$ (3 mL), **5**[23] (760 mg, 2.39 mmol), $Cu(OAc)_2$ (36.0 mg, 0.198 mmol) and sodium L-ascorbate (78.0 mg, 0.394 mmol) were added. The mixture was stirred at room temperature for 20 h. The residue was extracted with $CHCl_3$ (3 × 10 mL), and the organic phase was washed with water, dried over anhydrous $Na_2SO_4$ and concentrated. The crude product was purified by column chromatography using $CHCl_3$-MeOH as an eluent to give **7** (860 mg, 89%) as a light yellow waxy solid. $^1$H-NMR ($CDCl_3$, 500 MHz): δ 7.97 (s, 1H), 7.43 (s, 1H), 7.13 (s, 1H), 5.73 (s, 2H), 5.28 (br s, 1H), 4.57 (t, *J*=4.9 Hz, 2H), 3.88 (t, *J* =5.2 Hz, 2H), 3.64–3.57 (br m, 8H), 3.54 (t, *J*=5.4 Hz, 2H), 3.29 (q, *J*=5.2 Hz, 2H), 1.42 (s, 9H); HR-FAB-MS *m/z*: 470.2377 ([M+H]$^+$, calcd for $C_{19}H_{32}N_7O_7$: 470.2363).

**11-{4-[(2-Nitro-1*H*-imidazol-1-yl)methyl]-1*H*-1,2,3-triazol-1-yl}-3,6,9-trioxaundecan-1-amine trifluoroacetate (8):** To a solution of **7** (300 mg, 0.639 mmol) in $CH_2Cl_2$ (4 mL), TFA (1 mL) was added. The mixture was stirred at room temperature for 45 min and then quenched with water (10 mL). After extraction by $CHCl_3$ (2 × 5 mL). The aqueous layer was isolated and sodium hydroxide (40% aqueous solution) was added to pH 7–8 and extracted with $CHCl_3$ (3 × 15 mL). The organic layer was dried over anhydrous $MgSO_4$ and evaporated. The obtained product was purified by RP-MPLC using $H_2O$/MeCN containing 0.1% TFA as an eluent to give **8** (210 mg, 68%) as a waxy yellow solid. $^1$H-NMR ($CD_3OD$, 500 MHz): δ 8.17 (s, 1H), 7.66 (s, 1H), 7.24 (s, 1H), 5.83 (s, 3H), 5.81 (s, 2H), 4.63 (2H, t, *J*=4.5 Hz), 3.92 (2H, t, *J*=4.6 Hz), 3.77 (2H, t, *J*=4.6 Hz), 3.68–3.61 (m, 2H), 3.61 (br, 6H), 3.25 (2H, br s); HR-DART-MS *m/z*: 370.1843 ([M+H]$^+$, calcd for $C_{14}H_{24}N_7O_5$: 370.1839).

**Tricarbocyanine GPU-297:** Compound **8** (37.0 mg, 0.0765 mmol) was added to a solution of **1** (20.0 mg, 0.0267 mmol) in DMF (3 mL). The mixture was stirred at 80 °C for 4 h. After the solvent was removed, the residue was dissolved in MeOH (2 mL) and precipitated by $Et_2O$ (25 mL). The solid was collected by centrifugation and was further purified with RP-MPLC using 0.1 M $Et_3N$/AcOH buffer (pH 7.3)/MeCN as an eluent to give GPU-297 (17.6 mg, 61%) as a dark blue solid. $^1$H-NMR (DMSO-*d*$_6$, 500 MHz): δ 8.13 (s, 1H), 7.78 (s, 1H), 7.68 (d, *J*=12.6 Hz, 2H), 7.47 (d, *J*=7.4 Hz, 2H), 7.32 (t, *J*=7.6 Hz, 2H), 7.23 (s, 1H), 7.20 (d, *J*=7.8 Hz, 2H), 7.09 (t, *J*=7.4 Hz, 2H), 5.86 (d, *J*=10.5 Hz, 2H), 5.73 (s, 2H), 4.52 (t, *J*=5.1

Hz, 2H), 4.00 (br, 4H), 3.87 (br, 2H), 3.81 (t, *J*=5.1 Hz, 2H), 3.82–3.72 (m, 2H), 3.62–3.55 (m, 2H), 3.56–3.44 (m, 6H), 2.62–2.48 (m, 7H), 1.84–1.70 (m, 10H), 1.63 (s, 12H); HR-ESI-MS *m/z*: 1060.4666 ($[M+2H-Na]^+$, calcd for $C_{52}H_{69}N_9O_{11}S_2$: 1060.4631).

**Tricarbocyanine GPU-309:** Compound **8** (37.0 mg, 0.100 mmol) was added to a solution of **2** (13.0 mg, 0.0183 mmol) in DMF (3 mL). The mixture was stirred at 80 °C for 4 h. After the solvent was removed, the residue was dissolved in MeOH (2 mL) and precipitated by $Et_2O$ (25 mL). The solid was collected by centrifugation and was further purified with RP-MPLC using 0.1 M $Et_3N$/AcOH buffer (pH 7.3)/MeCN as an eluent to give GPU-309 (12.5 mg, 65%) as a dark blue solid. $^1$H-NMR (DMSO-*d*$_6$, 500 MHz): δ 8.08 (s, 1H), 7.71 (s, 1H), 7.67–7.59 (m, 4H), 7.58 (dd, *J*=8.3, 1.3 Hz, 2H), 7.17 (s, 1H), 7.05 (d, *J*=8.2 Hz, 2H), 5.78 (d, *J*=12.4 Hz, 2H), 5.68 (s, 2H), 4.48 (t, *J*=5.2 Hz, 2H), 3.99 (q, *J*=6.5 Hz, 4H), 3.84 (t, *J*=4.7 Hz, 2H), 3.78 (t, *J*=5.2 Hz, 2H), 3.73 (t, *J*=4.7 Hz, 2H), 3.62–3.4 (m, 8H), 2.52–2.46 (m, 4H), 1.79–1.68 (m, 2H), 1.60 (s, 12H), 1.23 (t, *J*=6.7 Hz, 6H); HR-ESI-MS *m/z*: 1004.4032 ($[M+2H-K]^+$, calcd for $C_{48}H_{61}N_9O_{11}S_2$: 1004.4005).

***tert*-Butyl [1-(2-nitro-1*H*-imidazol-1-yl)-2-oxo-6,9,12-trioxa-3-azatetradecan-14-yl]carbamate (11):** To a solution of **9**[26] (350 mg, 2.05 mmol) in DMF (4 mL), CDI (350 mg, 2.16 mmol) was added. The mixture was stirred at room temperature for 45 min. Compound **10**[25] (600 mg, 2.05 mmol) was added, and the mixture was stirred for 18 h at room temperature. DMF was removed and the residue was treated with water and extracted with $CHCl_3$, the combined organic extract was dried over anhydrous $MgSO_4$ and evaporated. The residue was purified by column chromatography using $CHCl_3$-MeOH as an eluent to give **11** (710 mg, 78%) as a yellow waxy solid. $^1$H-NMR ($CDCl_3$, 500 MHz): δ 7.64 (br s, 1H), 7.28 (s, 1H), 7.15 (s, 1H), 5.43 (t, *J*=5.4 Hz, 1H), 5.12 (s, 2H), 3.64 (s, 8H), 3.6–3.51 (m, 4H), 3.45 (q, *J*=5.2 Hz, 2H), 3.29 (q, *J*=5.4 Hz, 2H), 1.43 (s, 9H); HR-DART-MS *m/z*: 446.2290 ($[M+H]^+$, calcd for $C_{18}H_{32}N_5O_8$: 446.2251).

***N*-(11-Amino-3,6,9-trioxaundecyl)-2-(2-nitro-1*H*-imidazol-1-yl)acetamide trifluoroacetate (12):** To a solution of **11** (300 mg, 0.67 mmol) in $CH_2Cl_2$ (4 mL), TFA (1 mL) was added, the mixture was stirred at room temperature for 45 min and then quenched with water (10 mL). After extraction by $CHCl_3$ (2 × 5 mL). The aqueous layer was isolated and sodium hydroxide (40% aqueous solution) was added to pH 7–8 and then extracted with $CH_2Cl_2$ (3 × 20 mL). The organic layer was dried over anhydrous $MgSO_4$ and evaporated. The crude product which was purified by RP-MPLC using $H_2O$/MeCN containing 0.1% TFA as eluent to give **12** (190 mg, 61%) as a waxy yellow solid. $^1$H-NMR ($CDCl_3$, 500 MHz): δ 8.56 (t, *J*=5.4 Hz, 1H), 8.07 (br s, 3H), 7.64 (s, 1H), 7.18 (s, 1H), 5.15 (s, 2H), 3.64 (t, *J*=4.9 Hz, 2H), 3.59 (s, 4H), 3.56 (s, 4H), 3.46 (t, *J*=5.7 Hz, 2H), 3.29 (q, *J*=5.4 Hz, 2H), 3.05–2.97 (m, 2H); HR-DART-MS *m/z*: 346.1732 ([M-trifluoroacetate]$^+$, calcd for $C_{13}H_{24}N_5O_6$: 346.1727).

**Tricarbocyanine GPU-298:** Compound **12** (35.0 mg, 0.0762 mmol) was added to a solution of **1** (20.0 mg, 0.0267 mmol) in DMF (3 mL). The mixture was stirred at 80 °C for 4 h. After the solvent was removed, the residue was dissolved in MeOH and precipitated by $Et_2O$. The solid was collected by centrifugation and was further purified with RP-MPLC using 0.1 M $Et_3N$/AcOH buffer (pH 7.3)/MeCN as an eluent to give compound GPU-298 as a dark blue solid; yield (16.0 mg, 57%). $^1$H-NMR (DMSO-$d_6$, 500 MHz): δ 8.45 (t, *J*=5.7Hz, 1H), 7.65 (s, 1H), 7.62 (s, 2H), 7.43 (d, *J*=7.3 Hz, 2H), 7.28 (t, *J*=7.7 Hz, 2H), 7.19–7.14 (m, 3H), 7.05 (t, *J*=7.4 Hz, 2H), 5.82 (d, *J*=11.8 Hz, 2H), 5.09 (s, 2H), 3.95 (br t, *J*=6.1 Hz, 4H), 3.83 (br t, *J*=4.8 Hz, 2H), 3.73 (br t, *J*=4.6 Hz, 2H), 3.62–3.43 (m, 8H), 3.42 (m, 6H), 3.39 (t, *J*=5.8 Hz, 2H), 3.21 (q, *J*=5.7 Hz, 2H), 2.51–2.42 (m, 2H), 1.79–1.63 (m, 10H), 1.60 (s, 12H); HR-ESI-MS *m/z*: 1036.4546 ($[M+2H-Na]^+$, calcd for $C_{51}H_{69}N_7O_{12}S_2$: 1036.4518).

**Tricarbocyanine GPU-310:** Compound **12** (35.0 mg, 0.0762 mmol) was added to a solution of **2** (13.0 mg, 0.0183 mmol) in DMF (3 mL). The mixture was stirred at 80 °C for 4 h. After the solvent was removed in vacuo, the residue was dissolved in MeOH (2 mL) and precipitated by $Et_2O$ (25 mL). The solid was collected by centrifugation and was further purified with RP-MPLC using 0.1 M $Et_3N$/AcOH buffer (pH 7.3)/MeCN as an eluent to give GPU-310 (12.5 mg, 67%) as a dark blue solid. $^1$H-NMR (DMSO-$d_6$, 400 MHz): δ 8.44 (t, *J*=5.6 Hz, 1H), 7.67–7.59 (m, 5H), 7.56 (dd, *J*=8.2, 1.3 Hz, 2H), 7.16 (s, 1H), 7.06 (d, *J*=8.3 Hz, 2H), 5.79 (d, *J*=12.9 Hz, 2H), 5.08 (s, 2H), 3.99 (q, *J*=6.6 Hz, 4H), 3.84 (t, *J*=4.7 Hz, 2H), 3.74 (t, *J*=4.7 Hz, 2H), 3.64–3.47 (m, 8H), 3.41 (t, *J*=5.8 Hz, 2H), 3.22 (q, *J*=5.8 Hz, 2H), 2.49 (m, 4H), 1.78–1.68 (m, 2H), 1.60 (s, 12H), 1.21 (t, *J*=7.0 Hz, 6H); HR-ESI-MS *m/z*: 980.3912 ($[M+2H-K]^+$, calcd for $C_{47}H_{61}N_7O_{12}S_2$: 980.3892).

**Tricarbocyanine GPU-198:** To a solution of **13**[27] (87.5 mg, 0.101 mmol), DIC (23.0 μL, 0.147 mmol), HOSu (16.1 mg, 0.140 mmol), and DMAP (6.5 mg, 0.053 mmol) were dissolved in 4 mL of DMF and stirred at room temperature for 24 h. After $Et_2O$ (30 mL) was added to the mixture, the precipitated was collected by centrifugation. This crude activated ester intermediate as dark green powder (106.0 mg) was used in the next step without further purification.

To this intermediate, **3** (93.5 mg, 0.292 mmol) and *N*,*N*-diisopropylethylamine (130 μL, 0.746 mmol) in anhydrous DMF (3mL) was stirred at room temperature for 24 h. After $Et_2O$ (30 mL) was added to the mixture, the precipitated was collected by centrifugation. This crude product was further purified with RP-MPLC using $H_2O$/MeOH as eluent to give GPU-198 (41.6 mg, 36%) as a dark green powder. $^1$H-NMR (DMSO-$d_6$, 500 MHz): δ 9.01 (br s, 1H), 8.55 (d, *J*=13.7 Hz, 2H), 8.46 (br t, *J*=5.5 Hz, 1H), 7.77 (d, *J*=8.6 Hz, 2H), 7.59 (s, 1H), 7.52 (d, *J*=7.5 Hz, 2H), 7.44 (d, *J*=8.0 Hz, 2H), 7.38 (t, *J*=7.7 Hz, 2H), 7.33 (d, *J*=8.0 Hz, 2H), 7.22 (t, *J*=7.4 Hz, 2H), 7.19 (s, 1H), 6.39 (d, *J*=14.3 Hz, 2H), 5.97 (d, *J*=5.7 Hz, 1H), 4.48 (d, *J*=10.9 Hz, 1H), 4.39–4.32 (m, 2H), 4.19 (br t, *J*=6.9 Hz, 4H), 4.11 (br q, *J*=4.6 Hz, 1H),

3.48–3.35 (m, 2H), 3.17 (d, *J*=4.0 Hz, 2H), 3.17–3.05 (m, 2H), 3.08–2.96 (m, 1H), 3.0–2.86 (m, 1H), 2.79 (br t, *J*=5.9 Hz, 5H), 2.47 (t, *J*=7.4 Hz, 4H), 1.94 (br t, *J*=5.9 Hz, 2H), 1.84–1.62 (m, 10H), 1.39 (s, 12H). HR-ESI-MS *m/z*: 1110.4407 ([M+ 2H-Na]$^+$, calcd for $C_{57}H_{71}N_7O_{10}S_3$: 1110.4497).

***N*-({1-[2-Hydroxy-3-(2-nitro-1*H*-imidazol-1-yl)propyl]piperidin-4-yl}methyl)-3-(4-hydroxyphenyl)-propanamide (15):** To a solution of **14**[28] (70.0 mg, 0.266 mmol) in DMF (3 mL), a solution of **3** (as free base, 68.0 mg, 0.240 mmol) in DMF (1 mL) was added. The mixture was stirred for 20 h at room temperature. After the solvent was removed, the residue was partially purified by column chromatography using $CHCl_3$/MeOH as an eluent to afford crude **15** (84.9 mg, 82%) as a yellow solid. FAB-MS *m/z*: 432 ([M$^+$+H]).

**Tricarbocyanine GPU-212:** To a solution of **15** (60.0 mg, 0.139 mmol) in DMF (10 mL), NaH (60% in mineral oil) (3.7 mg, 0.15 mmol) was added. The mixture was stirred at room temperature for 30 min. Subsequently, **1** (63.0 mg, 0.0841 mmol) in DMF (0.5 mL) was added dropwise. The mixture was stirred at room temperature for 1 h, then the reaction was quenched with small piece of dry ice. After the solvent was removed, the residue was dissolved in MeOH (2 mL) and precipitated by $Et_2O$ (25 mL). The solid was filtered and further purified with RP-MPLC using 0.1 M $Et_3N$/AcOH buffer (pH 7.3)/MeCN as an eluent to give GPU-212 (21.0 mg, 22%) as a dark green solid. $^1$H-NMR (DMSO-*d*$_6$, 500 MHz): δ 7.82 (d, *J*=14.2 Hz, 2H), 7.74 (t, *J*=5.5 Hz, 1H), 7.56 (s, 1H), 7.48 (d, *J*=7.4 Hz, 2H), 7.39 (t, *J*=7.8 Hz, 2H), 7.36 (t, *J*=7.1 Hz, 2H), 7.21 (d, *J*=8.9 Hz, 2H), 7.19 (t, *J*=7.3 Hz, 2H), 7.14 (s, 1H), 7.05 (d, *J*=8.5 Hz, 2H), 6.22 (d, *J*=14.1 Hz, 2H), 4.66 (dd, *J*=13.6, 2.5 Hz, 1H), 4.19 (dd, *J*=13.7, 8.1 Hz, 1H), 4.13 (t, *J*=6.5 Hz, 4H), 3.99–3.89 (m, 1H), 3.51 (s, 1H), 2.92–2.84 (m, 1H), 2.86–2.77 (m, 3H), 2.78–2.67 (m, 6H), 2.53–2.45 (m, 6H), 2.33–2.15 (m, 4H), 1.82–1.65 (m, 10H), 1.48 (t, *J*=10.1 Hz, 2H), 1.26 (s, 12H), 1.2–1.15 (m, 2H); HR-ESI-MS *m/z*: 1122.5063 ([M+2H-Na]$^+$, calcd for $C_{59}H_{76}N_7O_{11}S_2$: 1122.5039).

**HPLC analysis**

Analytical HPLC was performed on a reverse phase column (Waters symmetry C18 (3.5 μm, 4.6 × 75 mm) using suitable eluent gradient system, fitted on Shimadzu LC-20AD pumps, SPD-M20A detectors, CTO-20A column oven (maintaining 40 °C), and LCMS solution system.

**Spectroscopic assessment**

**Measurement of extinction coefficients:** The extinction coefficients (ε) of GPU molecules were calculated according to the Lambert–Beer law. Absorption spectra of the samples were recorded in methanol.

**Fluorescence spectrophotometry:** Fluorescence spectra of GPU molecules were recorded in MeOH at 25 °C. The slit widths for excitation and emission were set to 5 and 10 nm, respectively.

**Measurement of fluorescence quantum yield:** The fluorescence quantum yield (Φfl) was determined by integrating the corrected emission spectra and comparing the results to those for NK-1511 in DMSO (Φfl

= 0.63)[35] or ICG in MeOH (Φfl = 0.04).[36] Under these conditions, quantum yields were calculated using the following equation.

$\Phi x/\Phi st = [Ast/Ax][nx^2/nst^2][Dx/Dst]$

st: standard, x: sample

A: absorbance at the excitation wavelength.

*n*: refractive index

D: area under the fluorescence spectra on an energy scale.

**Hydrophobicity index (Rm)**

Rm values were determined according to a literature procedure.[37] In brief, solutions of test compounds were applied to a reversed-phase thin-layer chromatography plate and developed in saturated chambers with a mobile phase (10% 5 mM sodium phosphate buffer, pH 7.4, and 90% MeOH). The separated spots were identified under visible light. The retention factor ($R_f$) values were obtained from the RP-TLC system, and Rm values were calculated using the equation: $Rm = Log (1/R_f - 1)$.

***In vitro* fluorescence assay of SUIT-2/HRE-Luc cells incubated under different oxygen conditions**

SUIT-2/HRE-Luc cells were constructed according to a published method.[33] In these cells, the HIF-1α stability is strictly regulated by the oxygen concentration (HIF-1α expression is undetectable under normoxic conditions but significantly increases under hypoxic conditions[33]). The cells were maintained at 37 °C in 5% FCS-Dulbecco's-modified Eagle's medium (Nacalai Tesque, Kyoto, Japan) supplemented with penicillin (100 units/mL) and streptomycin (100 μg/mL). Hypoxic cell cultures were obtained in 5% $CO_2$/0.1% $O_2$ in an INVIVO$_2$ 400 hypoxia workstation (Ruskinn Technology, Ltd., Bridgend, UK). GPU probes (10 mM in DMSO) were diluted to 0.02, 0.1, 0.5, and/or 2 mM with a medium containing 10% DMSO.

SUIT-2/HRE-Luc cells ($2 \times 10^5$ cells/well) were seeded in a six-well plate. The cells were preincubated under aerobic or hypoxic conditions for 4 h before adding 1/100 volume of GPU solution to the culture (final GPU molecules concentrations were 0.2, 1, 5, and/or 20 μM with 0.1% DMSO) and incubating for 30 min. The cells were then washed with fresh medium, incubated for 1 h in fresh medium to release the unbound GPU molecules from the cells, and suspended in 200 μL of radioimmunoprecipitation assay (RIPA) buffer. Fluorescence intensities were obtained for 150 μL of the suspensions in a 96-well plate using an Infinite® F500 microplate reader (Tecan, Männedorf, Switzerland). The excitation/emission filters used to measure the fluorescence intensity were 620/780 nm. The following conditions were used for image acquisition: exposure time = 1 sec, binning = medium (8), field of view = 19 × 19 cm, and

f/stop = 1. Statistical analysis was performed using the Student's *t*-test. Values of $P < 0.05$ were considered statistically significant.

***In vivo* and *ex vivo* bioluminescence imaging of SUIT-2/HRE-Luc subcutaneous tumors in a mouse xenograft model**

All animal experiments were performed with the approval of the Animal Ethics Committees of Tokyo Institute of Technology (No. 2010006) and in accordance with the Ethical Guidelines for Animal Experimentation of Tokyo Institute of Technology. Male Balb/c nu/nu were purchased from Oriental Yeast Co., Ltd (Tokyo, Japan). All experimental mice were at 6–10 weeks old. A-low fluorescence background diet was fed to experimental mice. SUIT-2/HRE-Luc cells suspended in PBS ($1.0 \times 10^6$ cells/20 μL) were mixed with an equal volume of Geltrex (Invitrogen, Carlsbad, CA, USA) and injected into both forelegs of seven-week-old male nude mice. Mice with subcutaneous tumors 5–15 mm in diameter were used for experiments.

For *in vivo* photon counting to assess bioluminescence, tumor-bearing mice were injected intraperitoneally with 200 μL of D-luciferin solution (10 mg/mL in PBS, Promega, Madison, WI, USA) and placed in an IVIS®-SPECTRUM instrument (Waltham, MA, USA). Bioluminescence images were acquired 20 min after intraperitoneal injection of D-luciferin. For *ex vivo* imaging, mice were sacrificed immediately after *in vivo* imaging and bioluminescence images of the bodies and their organs were obtained within 10 min of *in vivo* imaging. The following conditions were used for image acquisition: exposure time = 2 min, lamp level = high, binning = medium (8), field of view = 19 × 19 cm (for *in vivo*) and 12.9 × 12.9 cm (for *ex vivo*), and f/stop = 1. The bioluminescence was analyzed using Living Image 3.20 software (Caliper Life Sciences). The minimum and maximum photons/s/cm$^2$/steradian of each image were indicated in each figure by a red bar scale.

GPU molecules (10 nmol) in 100 μL of PBS (pH 8.0) containing 0.2% DMSO was intravenously injected into tumor-bearing mice. *In vivo* fluorescence images were acquired at indicated times. For *ex vivo* imaging, mice were sacrificed after *in vivo* imaging and their organs were harvested. All fluorescence images were acquired with an IVIS®-SPECTRUM instrument using the same parameters for the excitation filter (640 nm for GPU-210; 675 nm for GPU-297; 710 nm for GPU-316), emission filter (760 nm for GPU-210 and GPU-297; 800 nm for GPU-316), and exposure time (1 sec); binning = medium (8), field of view = 19 × 19 cm, f/stop = 1. No subtraction was performed to remove the background signal after fluorescence imaging acquisition.

**Analysis of T/B ratio:** The photon flux/sec in the same areas (region of interest: ROI) of the tumors and the muscles in the lower limbs was counted at the indicated time after GPU molecules injection. Each photon flux/sec value was normalized by subtracting the background photon flux/sec in the corresponding ROI. T/B was calculated by dividing the normalized values in tumors by those in the muscle.

## ACKNOWLEDGEMENTS

This research was supported in part by a Grant from the Saijiro Endo Memorial Foundation for Science & Technology (to K.O.), a Grant-in-Aid for Young Scientists (B) (22790042 to K.O.), a Grant-in-Aid for Scientific Research on Priority Areas (20011009 to H.N.) from the Japan Society for the Promotion of Science, and a Grant-in-Aid for Scientific Research on Innovative Areas "Integrative Research on Cancer Microenvironment Network" (22112009 to S.K.K.) from the Ministry of Education, Culture, Sports, Science, and Technology of Japan.

## REFERENCES

1. V. Bhandari, C. Hoey, L. Y. Liu, E. Lalonde, J. Ray, J. Livingstone, R. Lesurf, Y.-J. Shiah, T. Vujcic, X. Huang, S. M. G. Espiritu, L. E. Heisler, F. Yousif, V. Huang, T. N. Yamaguchi, C. Q. Yao, V. Y. Sabelnykova, M. Fraser, M. L. K. Chua, T. van der Kwast, S. K. Liu, P. C. Boutros, and R. G. Bristow, *Nat. Genet.*, 2019, **51**, 308.
2. V. Petrova, M. Annicchiarico-Petruzzelli, G. Melino, and I. Amelio, *Oncogenesis*, 2018, **7**, 10.
3. B. Muz, P. de la Puente, F. Azab, and A. K. Azab, *Hypoxia (Auckl)*, 2015, **3**, 83.
4. A. Challapalli, L. Carroll, and E. O. Aboagye, *Clin. Transl. Imaging*, 2017, **5**, 225.
5. R. Kumari, D. Sunil, R. S. Ningthoujam, and N. A. Kumar, *Chem. Biol. Interact.*, 2019, **307**, 91.
6. S. Kizaka-Kondoh and H. Konse-Nagasawa, *Cancer Sci.*, 2009, **100**, 1366.
7. J. A. Raleigh, S.-C. Chou, G. E. Arteel, and M. R. Horsman, *Radiat. Res.*, 1999, **151**, 580.
8. J. G. Rajendran and K. A. Krohn, *Semin. Nucl. Med.*, 2015, **45**, 151.
9. P. J. Cassidy and G. K. Radda, *J. R. Soc. Interface*, 2005, **2**, 133.
10. Y. Wu, W. Zhang, J. Li, and Y. Zhang, *Am. J. Nucl. Med. Mol. Imaging*, 2013, **3**, 1.
11. S. Luo, E. Zhang, Y. Su, T. Cheng, and C. Shi, *Biomaterials*, 2011, **32**, 7127.
12. K. Okuda, Y. Okabe, T. Kadonosono, T. Ueno, B. G. M. Youssif, S. Kizaka-Kondoh, and H. Nagasawa, *Bioconjug. Chem.*, 2012, **23**, 324.
13. B. G. M. Youssif, K. Okuda, T. Kadonoso, O. I. A. R. Salem, A. A. M. Hayallah, M. A. Hussein, S. Kizaka-Kondoh, and H. Nagasawa, *Chem. Pharm. Bull.*, 2012, **60**, 402.
14. H. Lee, J. C. Mason, and S. Achilefu, *J. Org. Chem.*, 2006, **71**, 7862.
15. N. Narayanan and G. Patonay, *J. Org. Chem.*, 1995, **60**, 2391.
16. X. Peng, F. Song, E. Lu, Y. Wang, W. Zhou, J. Fan, and Y. Gao, *J. Am. Chem. Soc.*, 2005, **127**, 4170.
17. I. Mohammad, C. Stanford, M. D. Morton, Q. Zhu, and M. B. Smith, *Dyes Pigm.*, 2013, **99**, 275.
18. J. H. Flanagan, S. H. Khan, S. Menchen, S. A. Soper, and R. P. Hammer, *Bioconjug. Chem.*, 1997, **8**, 751.

19. F. Song, X. Peng, E. Lu, R. Zhang, X. Chen, and B. Song, *J. Photochem. Photobiol. A*: *Chem.*, 2004, **168**, 53.
20. K. Tsuchikama and Z. An, *Protein Cell*, 2018, **9**, 33.
21. J. F. Bunnett, *Acc. Chem. Res.*, 1978, **11**, 413.
22. H. C. Kolb and K. B. Sharpless, *Drug Discov. Today*, 2003, **8**, 1128.
23. T. K. Neklesa, H. S. Tae, A. R. Schneekloth, M. J. Stulberg, T. W. Corson, T. B. Sundberg, K. Raina, S. A. Holley, and C. M. Crews, *Nat. Chem. Biol.*, 2011, **7**, 538.
24. R. Bejot, L. Carroll, K. Bhakoo, J. Declerck, and V. Gouverneur, *Bioorg. Med. Chem.*, 2012, **20**, 324.
25. W. Zhang, D. T. Nowlan, L. M. Thomson, W. M. Lackowski, and E. E. Simanek, *J. Am. Chem. Soc.*, 2001, **123**, 8914.
26. J. M. Khurana, S. Chauhan, and G. Bansal, *Monatsh. Chem.*, 2004, **135**, 83.
27. W. Wang, S. Ke, S. Kwon, S. Yallampalli, A. G. Cameron, K. E. Adams, M. E. Mawad, and E. M. Sevick-Muraca, *Bioconjug. Chem.*, 2007, **18**, 397.
28. C. Li, T. R. Greenwood, Z. M. Bhujwalla, and K. Glunde, *Org. Lett.*, 2006, **8**, 3623.
29. H. van de Waterbeemd, D. A. Smith, and B. C. Jones, *J. Comput. Aided Mol. Des.*, 2001, **15**, 273.
30. B. E. Schaafsma, J. S. D. Mieog, M. Hutteman, J. R. van der Vorst, P. J. K. Kuppen, C. W. G. M. Löwik, J. V. Frangioni, C. J. H. van de Velde, and A. L. Vahrmeijer, *J. Surg. Oncol.*, 2011, **104**, 323.
31. N. C. Biswal, C. Pavlik, M. B. Smith, A. Aguirre, Y. Xu, S. Zanganeh, L. T. Kuhn, K. P. Claffey, and Q. Zhu, *J. Biomed. Opt.*, 2011, **16**, 066009.
32. N. Onda, M. Kimura, T. Yoshida, and M. Shibutani, *Int. J. Cancer*, 2016, **139**, 673.
33. S. Kizaka-Kondoh, S. Itasaka, L. Zeng, S. Tanaka, T. Zhao, Y. Takahashi, K. Shibuya, K. Hirota, G. L. Semenza, and M. Hiraoka, *Clin. Cancer Res.*, 2009, **15**, 3433.
34. T. Kuchimaru, T. Kadonosono, S. Tanaka, T. Ushiki, M. Hiraoka, and S. Kizaka-Kondoh, *PLoS ONE*, 2010, **5**, e15736.
35. R. C. Benson and H. A. Kues, *J. Chem. Eng. Data*, 1977, **22**, 379.
36. S. A. Soper and Q. L. Mattingly, *J. Am. Chem. Soc.*, 1994, **116**, 3744.
37. M. das G. Cardoso, D. L. Nelson, A. T. do Amaral, C. D. dos Santos, A. de. A. Pereira, and A. C. B. de Oliveira, *Int. J. Mol. Sci.*, 2002, **3**, 755.